Supporting Information

Manuscript ID: CC-COM-10-2023-005365.R1

Title: Interfacial Engineering of Si Anodes by Confined Doping of Co toward High Initial Coulombic Efficiency

Yuanyuan Han[1,#], Haoyu Fu[1,#], Guihuan Chen[1,], Xiaoshan Wang[1], Yue Zhao[1], Xiang Sui[1], Zhiqiang Zhao[1], Xiancheng Sang[1], Qinghao Li[1], and Qiang Li[1,*]*

[1] College of Physics, Weihai Innovation Research Institute, College of Materials Science and Engineering, Qingdao University, Qingdao 266071, China

# These authors contributed to this work equally.

* Corresponding author E-mail addresses: liqiang@qdu.edu.cn (Q. Li), and chenguihuan@qdu.edu.cn.

The Supporting information include:

Section S1. Experimental section

Preparation of Si-Co alloy thin film electrode

The multilayer films were prepared by alternating magnetron sputtering with 5×10^{-8} supporting pressure as base pressure at room temperature. Under 7.5 mTorr argon pressure, the silicon cobalt film (purity of 99.99%) was deposited on the copper foil by alternating RF sputtering and DC sputtering. The growing power of Si and Co targets is 120W and 30W, respectively. During alternating sputtering, substrate rotation is employed to ensure film uniformity. Similarly, Si/Si-Co alloy film anodes with different components were prepared by controlling alternating magnetron sputtering power and time. The anodes were named Si/Si-Co-3, Si/Si-Co-5, Si/Si-Co-10, and Si/Si-Co-20, denoting different cobalt component contents (Table S1). The marked numbers are cobalt atomic layer content (unit: Å). In addition, for the deposition of Si amorphous cathode, the growth power of Si target layer is 120W.

Material characterization

The crystal structure of the resulting films was characterized by X-ray diffraction (XRD, Bruker D8 advance) with Cu Kα radiation. The thicknesses of films were measured by an Atomic Force Microscope (AFM, PARK XE7) X-ray photoelectron spectroscopy (XPS) analysis was carried out on a Thermo Scientific ESCALAB 250XI photoelectron spectrometer. Scanning electron microscopy (SEM, JSM-6700F), transmission electron microscopy (TEM, JEM-2100F), Energy Dispersive X-ray spectroscopy (EDX) mapping images were used to study the morphology and structure of the samples. Electron Paramagnetic Resonance (EPR) spectra were collected on EMXplus-6/1/P/L EPR spectrometer.

Electrochemical test

The electrochemical performance of Si/Si-Co anode was studied by assembling a half-cell in argon-filled glove box. The electrolyte used in this experiment was 1 mol/L $LiPF_6$ in the mixed solution of Ethyl Methyl Carbonate (EMC) and Fluoroethylene carbonate (FEC) at a volume ratio of 3:7. Cyclic voltammetry (CV) was performed at various scanning rates between 0.01 and 2.00 V (versus Li^+/Li) on a CHI660E electrochemical workstation. On Land battery test system (Land, CT2001A), constant

current charge and discharge tests are performed with different current densities in the cut-off voltage range of 0.01~2.0V. The galvanostatic intermittent titration technique (GITT) test was conducted on a Land Battery Tester. All electrochemical tests were performed at room temperature.

Magnetic measurement.

The battery for the in situ and non-in situ magnetic measurement are assembled/unpacked at room temperature in a glove box filled with argon gas to exclude influences other than the electrodes themselves. Magnetic measurements were performed on a physical property measurement system (PPMS, Quantum Design) using the self-developed batteries for the in situ measurements.[1-7] The magnetic hysteresis (MH) curve magnetic measurements on the electrode materials were carried out ex situ, the electrodes were washed in the glovebox after being discharged to 0.01 V to avoid oxidation, and 0-3 T magnetic field was selected for MH at room temperature. All operando magnetization measurements were carried out simultaneously with electrochemical discharge-charge processes under magnetic fields parallel to the copper foil.

Section S2. Supplementary tables

Table S1. Different proportions of Si/Si-Co thin film electrodes

Film	Power (W)	Si Thickness(Å)	Co Thickness(Å)	layer
Si/Si-Co-3	Co 30W Si 120W	100	3	30
Si/Si-Co-5	Co 30W Si 120W	100	5	30
Si/Si-Co-10	Co 30W Si 120W	100	10	30
Si/Si-Co-20	Co 30W Si 120W	100	20	30

Section S3. Supplementary Figures

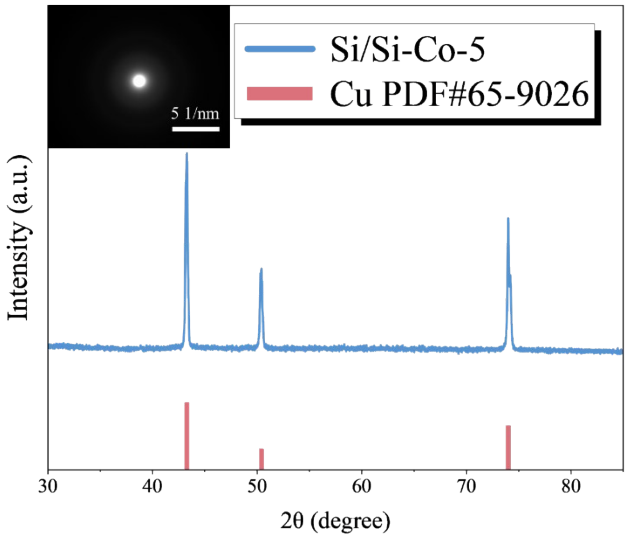

Fig. S1 XRD pattern of Si/Si-Co-5 thin film (inset shows SAED pattern of Si/Si-Co-5).

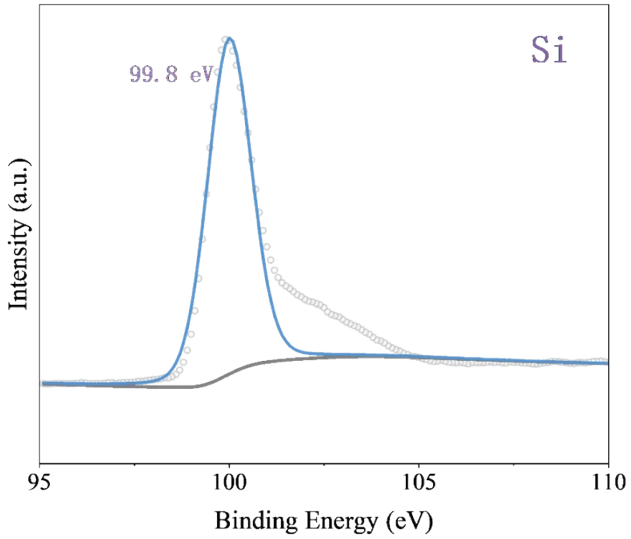

Fig. S2 XPS nuclear grade Si 1s spectra of original Si/Si-Co-5 samples

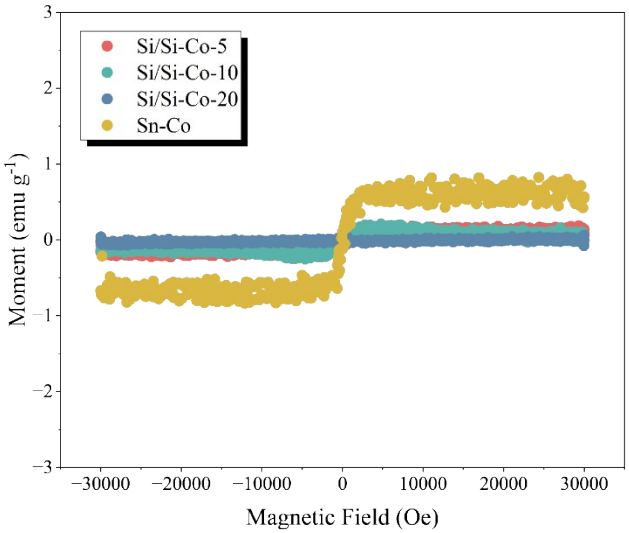

Fig. S3 Magnetic measurements of different anode materials at initial state.

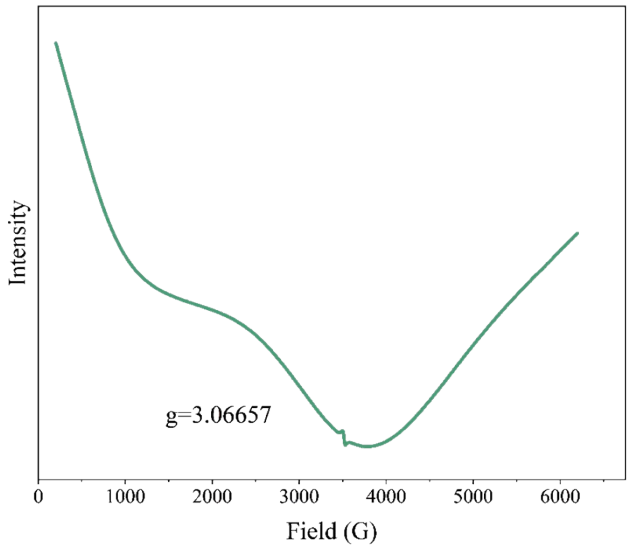

Fig. S4 EPR spectra of Co.

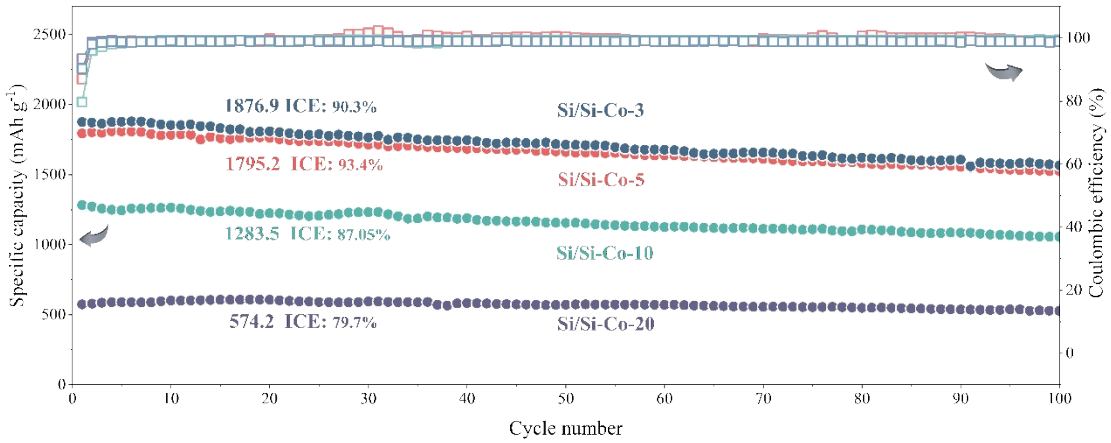

Fig. S5 Cycling properties of Si/Si-Co films with different cobalt content.

Fig. S5 shows the long-term cyclic charge-discharge properties of Si/Si-Co films with different cobalt content, accompanied by the initial Coulomb efficiency. It is observed that Co decoration can increase the ICE significantly, and the sample with Co coating amount of 0.3-1nm (each alternate layer) deliver similar ICE values, while excessive Co coating(with 2nm each alternate layer) leads to a lowered value. This is because the large amount of cobalt deposition may alienate the contact between Co and Si, and the effective contact area may be reduced, so that its role can not be fully played. The lower deposition amount (with 0.3nm Co coating) resultes in inadequate alloying with sillion, leading to lower ICE values.

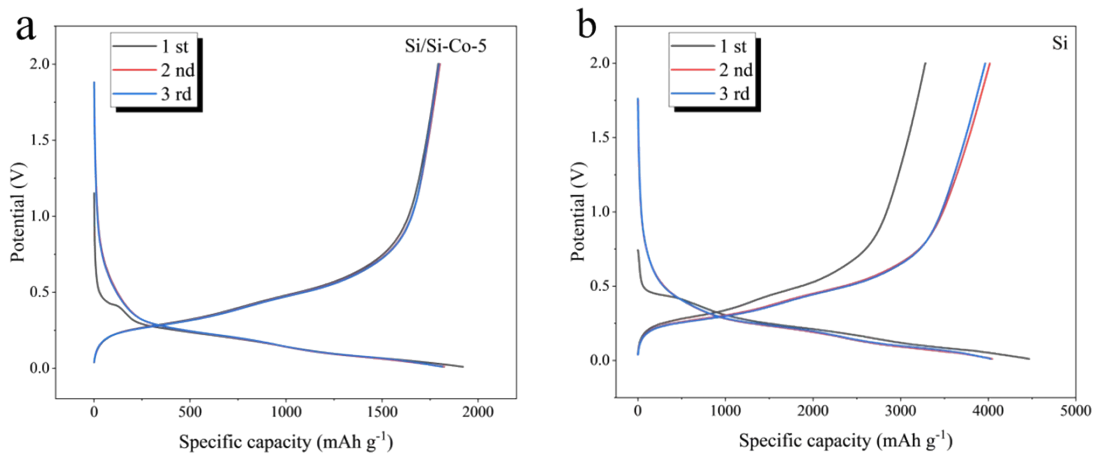

Fig. S6 Voltage-capacity diagram of (a) Si/Si-Co-5, (b) Si

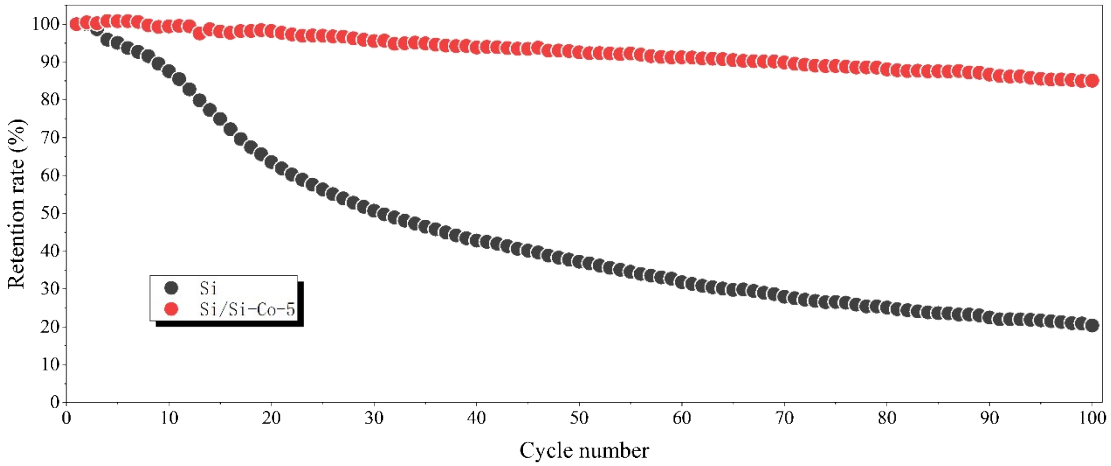

Fig. S7 Comparison of capacity retention rates of Si films and Si/Si-Co-5 films.

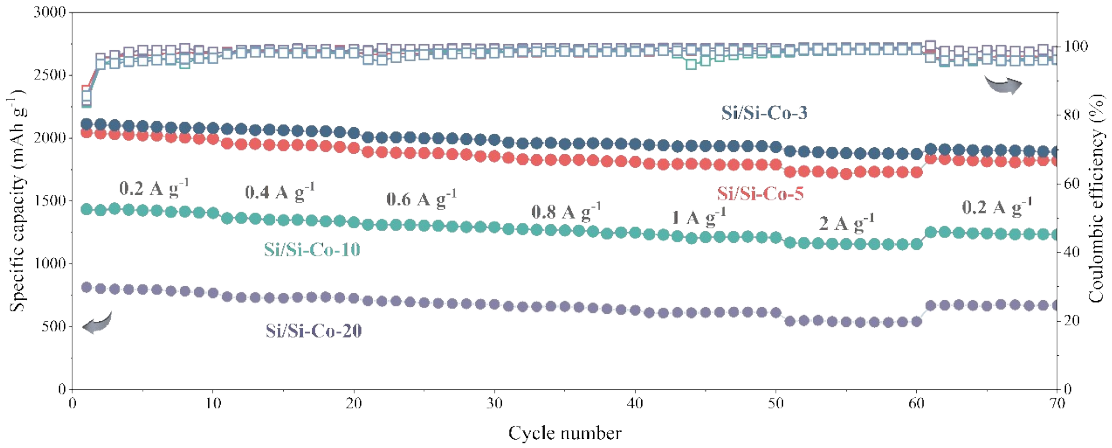

Fig. S8 Rate performances of Si/Si-Co films with different Co content.

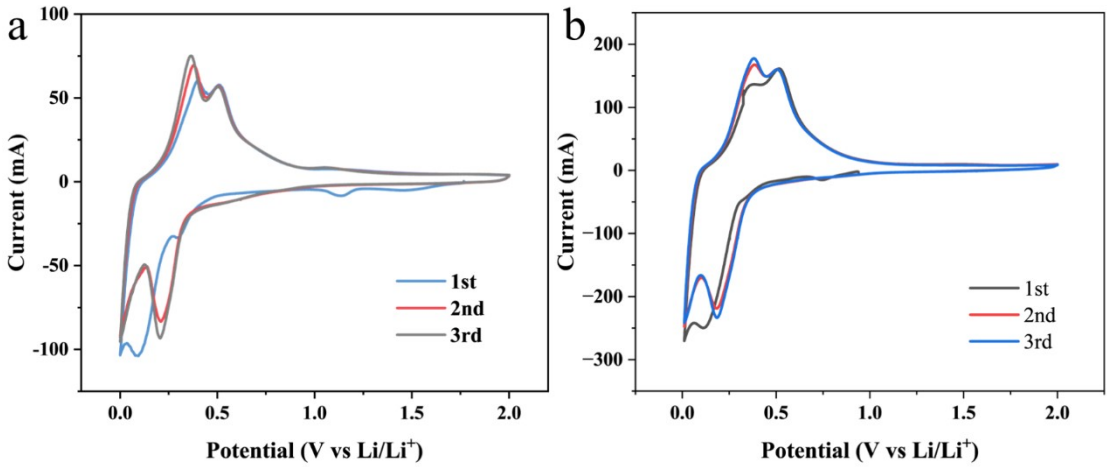

Fig. S9 (a) CV curves of Si/Si-Co-5 with a scan rate of 0.5 mV s^{-1} at 3 Tesla applied magnetic field, and (b) CV curve of Si/Si-Co-5 in the button battery at a scanning rate of 0.5 mV s^{-1}.

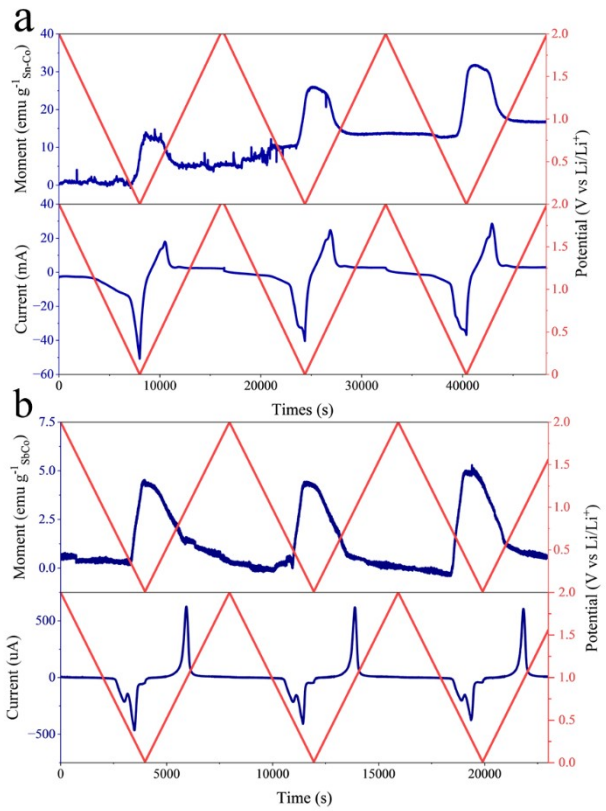

Fig. S10 Charge-discharge profiles and the corresponding magnetization variations. of (a) SnCo LIBs and (b) SbCo LIBs.

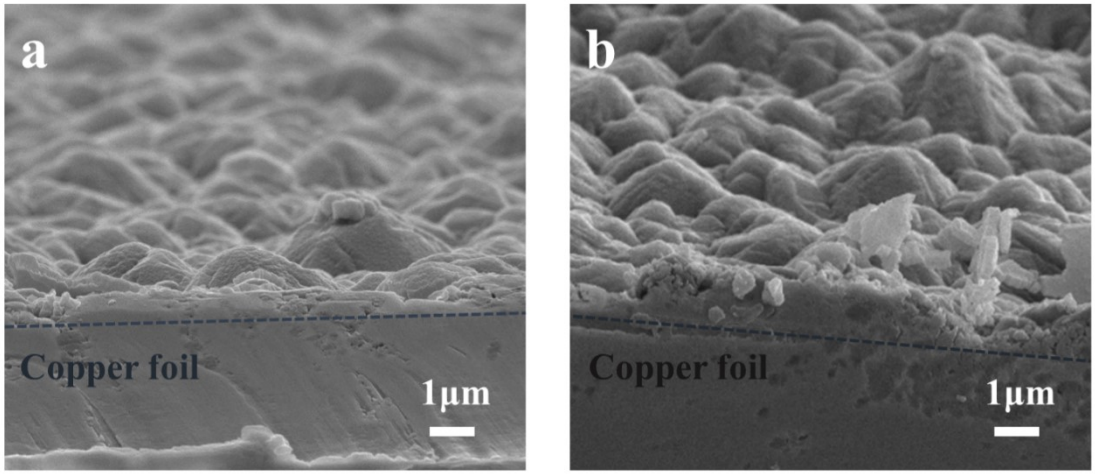

Fig. S11 SEM images of the cross-section of Si/Si-Co-5 films (a) before and (b) after battery cycling.

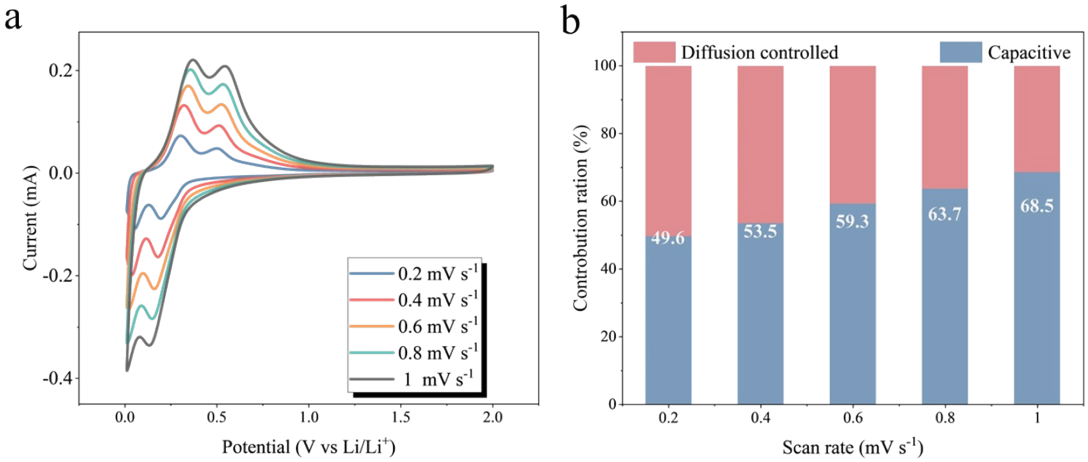

Fig. S12 (a) CV curves of Si/Si-Co-5 at current densities of 0.2, 0.4, 0.6, 0.8, and 1 mv s^{-1}, respectively. (b) Capacitance contribution of Si/Si-Co-5 at different scanning rates.

CV curves of Si/Si-Co-5 at different current densities were measured, as shown in **Fig. S10**, to gain insight into the kinetic features. The formula for calculating the pseudo capacitance effect on the electrode surface is as follows[8]：

$$i(V) = k_1 v + k_2 v^{\frac{1}{2}} \tag{1}$$

For ease of calculation, the above formula is converted to:

$$\frac{i(V)}{v^{\frac{1}{2}}} = k_1 v^{\frac{1}{2}} + k_2 \tag{2}$$

Where $i(V)$, $k_1 v$ and $k_2 v^{\frac{1}{2}}$ are the total current, the current generated by the pseudo-capacitance effect and the current generated by the diffusion control, respectively. The pseudo-capacitance contribution at different scanning rates is shown in **Fig. S10b**, the contribution (area) of the pseudo-capacitor is 49.6% at a low scan rate of 0.02 mV s^{-1}, while the contribution of the pseudo-capacitor rises significantly to 68.5% at a high scan rate of 1.0 mV s^{-1}. The results show that as the scanning rate increases, the CV shape of Si/Si-Co-5 anode is similar to the typical peak, indicating that the pseudo-capacitance effect is significant and the capacity at a specific voltage during the cycle is composed of capacitance control process and diffusion control process.

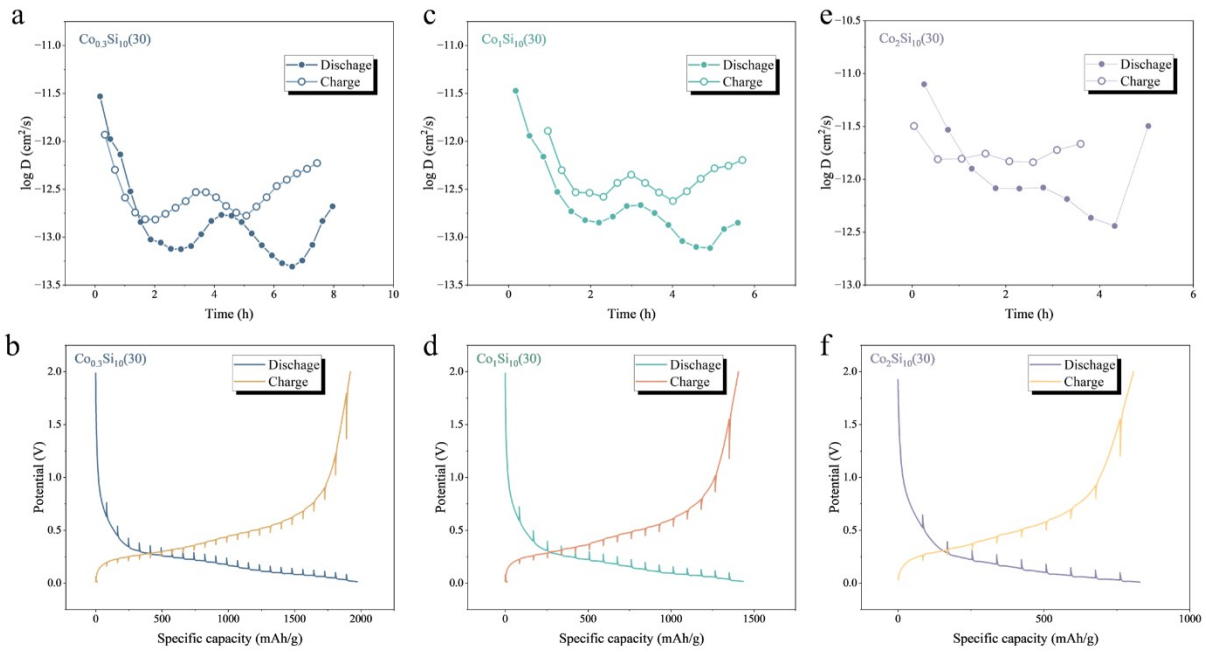

Fig. S13 Li^+ diffusion coefficient (a) Si/Si-Co-3 (30), (c) Si/Si-Co-10 (30) and (e) Si/Si-Co-20 anode; GITT curve (b) Si/Si-Co-3, (d) Si/Si-Co-10 and (f) Si/Si-Co-20 anode.

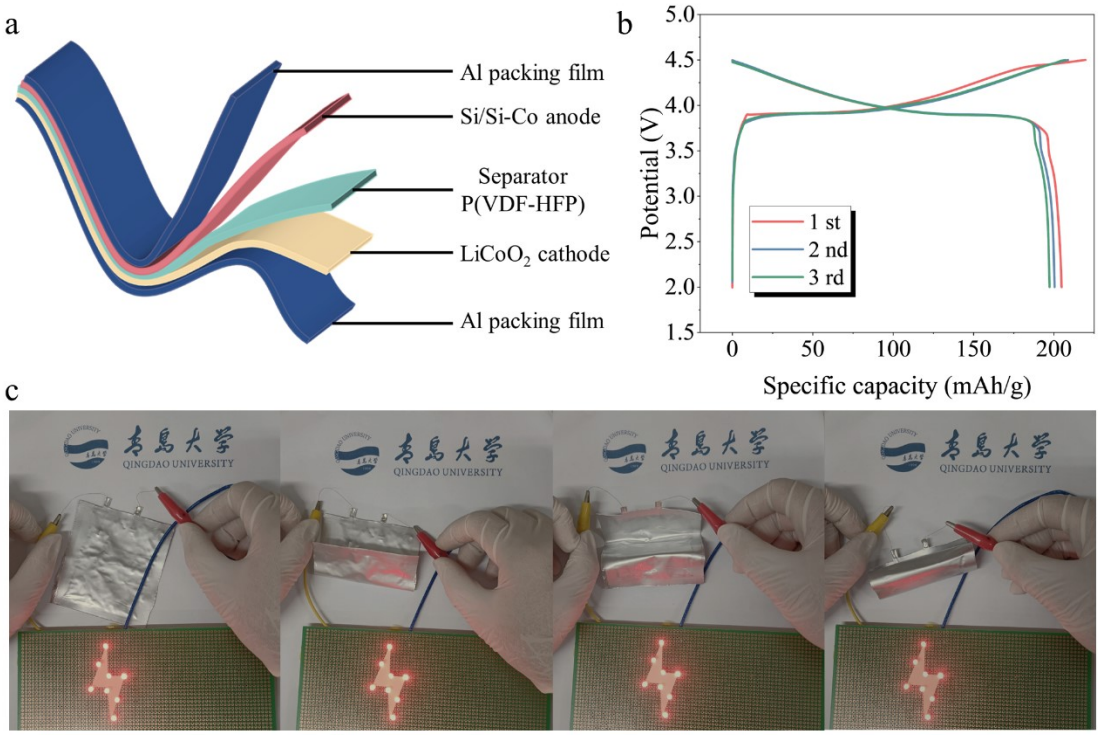

Fig. S14 (a) Schematic diagram of structure model of thin film battery. (b) Voltage-capacity diagram of Si/Si-Co-5 | P (VDF HFP) | $LiCoO_2$. (c)Working state of flexible quasi-solid state battery under different bending degrees.

Reference

1. Q. Li, H. Li, Q. Xia, Z. Hu, Y. Zhu, S. Yan, C. Ge, Q. Zhang, X. Wang, X. Shang, S. Fan, Y. Long, L. Gu, G. X. Miao, G. Yu and J. S. Moodera, *Nat. Mater.* , 2021, **20**, 76-83.
2. F. Zhang, Z. Li, Q. Xia, Q. Zhang, C. Ge, Y. Chen, X. Li, L. Zhang, K. Wang, H. Li, L. Gu, S. Yan, G.-X. Miao and Q. Li, *Matter*, 2021, **4**, 3605-3620.
3. Z. Li, Y. Zhang, X. Li, F. Gu, L. Zhang, H. Liu, Q. Xia, Q. Li, W. Ye, C. Ge, H. Li, H. Hu, S. Li, Y. Z. Long, S. Yan, G. X. Miao and Q. Li, *J. Am. Chem. Soc*, 2021, **143**, 12800-12808.
4. X. Li, J. Su, Z. Li, Z. Zhao, F. Zhang, L. Zhang, W. Ye, Q. Li, K. Wang, X. Wang, H. Li, H. Hu, S. Yan, G.-X. Miao and Q. Li, *Sci. Bull.*, 2022, **67**, 1145-1153.
5. X. Li, Z. Li, Y. Liu, H. Liu, Z. Zhao, Y. Zheng, L. Chen, W. Ye, H. Li and Q. Li, *Chin. J. Catal.*, 2022, **43**, 158-166.
6. H. Liu, F. Gu, X. Sang, Y. Han, F. Zou, Z. Li, Y. Qin, L. Cai, Y. Pan, Q. Cao, G.-x. Miao and Q. Li, *Phys. Rev. Appl.* , 2023, **19**, 054022.
7. H. Li, Z. Hu, Q. Xia, H. Zhang, Z. Li, H. Wang, X. Li, F. Zuo, F. Zhang, X. Wang, W. Ye, Q. Li, Y. Long, Q. Li, S. Yan, X. Liu, X. Zhang, G. Yu and G. X. Miao, *Adv Mater*, 2021, **33**, e2006629.
8. H. Yang, W. Kong, J. Yin, W. Feng, S. Xu, L. Cui and Z. Wen, *Surf. Interfaces*, 2021, **26**, 101435.